Contents lists available at ScienceDirect

Image and Vision Computing

journal homepage: www.elsevier.com/locate/imavis

Robust iris segmentation on uncalibrated noisy images using mathematical morphology

Miguel A. Luengo-Oroz [a,d,*], Emmanuel Faure [b,d], Jesús Angulo [c]

[a] Biomedical Image Technologies Lab of ETSI Telecomunicación, Universidad Politécnica de Madrid, Av. Complutense SN, 28040 Madrid, Spain
[b] Centre de Recherche en Epistémologie Applique, CNRS – École Polytechnique, 1 rue Descartes, 75005 Paris, France
[c] Centre de Morphologie Mathématique, Mathématiques et Systèmes, MINES Paristech, 35 rue Saint Honoré, 77300 Fontainebleau, France
[d] Complex Systems Institute of Paris, ISC-PIF, 57–59 rue Lhomond, 75005 Paris, France

A R T I C L E   I N F O

A B S T R A C T

This paper proposes a new approach for fast iris segmentation that relies on the closed nested structures of iris anatomy (the sclera is brighter than the iris, and the iris is brighter than the pupil) and on its polar symmetry. The described method applies mathematical morphology for polar/radial-invariant image filtering and for circular segmentation using shortest paths from generalized grey-level distances. The proposed algorithm obtained good results on the NICE-I contest and showed a very robust behavior, especially when dealing with half-closed eyes, different skin colours/illumination or subjects wearing glasses.

1. Introduction

Iris recognition is accepted as one of the best biometric features for individual identification due to several inherent properties of iris patterns, i.e., stability in lifetime, selectivity and reliability. In addition, acquisition of iris images is non-invasive and quite flexible even in non-collaborative frameworks. Nevertheless, as a first step, the accuracy of iris recognition depends not only on the quality of the images but also on the image segmentation algorithm which should extract the effective image region associated exclusively with the iris. To be integrated in an iris recognition system, the iris segmentation algorithm must be fast (i.e., segmentation is only a preprocessing step, and the feature extraction and database matching/classification are then the subsequent steps), and must be robust. Robustness involves, on the one hand, an algorithm which deals with the different noise factors (specular reflections, obstructions due to eyelashes, eyelids, glasses, etc.) and on the other hand, an algorithm defined by a reduced number of parameters. For an exhaustive and recent state-of-the-art on iris segmentation, the reader is invited to see the paper by Matey [1]. Despite all these constraints, the eye presents an interesting morphology of its anatomical elements: polar symmetry of iris and pupil, and closed nested structures of monotone decreasing intensities (the sclera is always brighter than the iris, and the iris is always brighter than the pupil). We have recently studied the application of

mathematical morphology to these kind of structures for polar/radial-invariant image filtering and feature extraction [2] and for circular segmentation using shortest paths from generalized grey-level distances [3], but in other application fields (quantitative cytology and spots of DNA microarray images). Motivated by the Noisy Iris Challenge Evaluation – Part I (NICE-I) [4] and by our previous works on cyclic mathematical morphology, we developed a robust and fast algorithm to perform segmentation of the noise-free iris regions acquired at the visible wavelength, on-the-move, at-a-distance, with minor cooperation and within dynamic imaging environments. The rest of the paper is organized as follows. A review on the used morphological tools is given in Section 2. Section 3 describes the different steps of the proposed algorithm. In Section 4, results of our approach on the NICE-I datasets are discussed. Conclusions are presented in Section 5.

2. Mathematical foundations of related morphological tools

Mathematical morphology is a nonlinear image processing methodology based on the application of lattice theory to spatial structures [5]. In this section, we briefly review the basic morphological operators and remind other less extended operators which are the basic ingredients of our iris segmentation algorithm.

2.1. Basic operators

In the framework of digital grids, a *grey tone image* can be represented by a function $f : D_f \to T$, where D_f is a subset of Z^2 and $T = \{t_{min}, \ldots, t_{max}\}$ is an ordered set of grey-levels, i.e., a subset of

* Corresponding author. Tel.: +34 913366827; fax: +34 913367323.
   E-mail addresses: maluengo@die.upm.es (M.A. Luengo-Oroz), emmanuel.faure @polytechnique.edu (E. Faure), jesus.angulo@mines-paristech.fr (J. Angulo).

Z. $f(\mathbf{x})$ is the grey value of the image at point $\mathbf{x} = (x, y)$. A *section of f* at level h (or, the threshold of f at value h) is a *set* $X_h(f)$ (compact set, $X_h : D_f \rightarrow \{0, 1\}$) defined as $X_h(f) = \{\mathbf{x} \in D_f : f(\mathbf{x}) \geqslant h\}$. The basic morphological operators are the dilation: $\delta_B(f(\mathbf{x})) = \sup_{\mathbf{y} \in B}\{f(\mathbf{x} - \mathbf{y})\}$ and the erosion: $\varepsilon_B(f(\mathbf{x})) = \inf_{-\mathbf{y} \in B}\{f(\mathbf{x} - \mathbf{y})\}$, where B be a subset of Z^2 and λ a scaling factor. λB is called *structuring element B* of size λ. The two elementary operations of *erosion* and *dilation* can be composed together giving the opening: $\gamma_B(f) = \delta_B[\varepsilon_B(f)]$ and the closing: $\varphi_B(f) = \varepsilon_B[\delta_B(f)]$. The morphological *openings* $\gamma_{\lambda B}$(*closings* $\varphi_{\lambda B}$) filter out light (dark) structures from the image according to a predefined size λ and shape criterion B.

2.2. Geodesic reconstruction, close-hole operator and area opening

A morphological tool that complements the opening and closing operators for feature extraction (extract the marked particles) is the morphological reconstruction, implemented using the *geodesic dilation* operator based on restricting the iterative dilation of a function marker f by B to a function mask or reference g, $\delta_g^n(f) = \delta_g^1 \delta_g^{n-1}(f)$, where $\delta_g^1(f) = \delta_B(f) \wedge g$. The *reconstruction* by dilation is defined by $\gamma^{rec}(g, f) = \delta_g^i(f)$, such that $\delta_g^i(f) = \delta_g^{i+1}(f)$ (idempotence). In particular, the *opening by reconstruction* is defined via the geodesic dilation using an opening as marker, i.e., $\gamma_\lambda^{rec}(f) = \gamma^{rec}(f, \gamma_\lambda(f)) = \gamma^{rec}(f, \varepsilon_\lambda(f))$. Using the geodesic reconstruction we can also define an operator to fills all holes in an image f that does not touch the image boundary f_∂ (used as a marker) and therefore provides a parameter free approach to detect holes in an image, i.e., $\psi^{ch}(f) = [\gamma^{rec}(f^c, f_\partial)]^c$, where f^c is the complement image (i.e., the negative). For a binary image, the definition of grains and holes is clear, for the case of grey-level images, a "hole" is defined as a set of connected points surrounded by connected components of value strictly greater than the hole values. This *close-holes operator* is a morphological closing and therefore removes the dark structures (valleys of intensity).

In general, we must notice that the *filters by reconstruction* involve the notion of connectivity (and preserve the "edges" of the structures), i.e., if X is connected, $\gamma_\lambda(X) \neq \emptyset \iff \gamma_\lambda^{rec}(X) = X$, and for functions, the opening by reconstruction is given by: $\gamma_\lambda^{rec}(f)(\mathbf{x}) = \sup\{h \leqslant f(\mathbf{x}) | \gamma_\lambda(\gamma_{\mathbf{x}}^c(X_h(f))) \neq \emptyset\}$, where $\gamma_{\mathbf{x}}^c(A)$ is the connected component of A marked by $\mathbf{x}$ (extracts the connected set containing $\mathbf{x}$). *Area opening* is a particular connected operator based on the notion of surface area [6]. The grey tone area opening of f of size λ_a, denoted $\gamma_{\lambda_a}^a(f)$, is given by: $\gamma_{\lambda_a}^a(f)(\mathbf{x}) = \sup\{h \leqslant f(\mathbf{x}) | A(\gamma_{\mathbf{x}}^c(X_h(f))) \geqslant \lambda_a\}$, where $A(X)$ is the area of X. The area opening can be seen as an opening with a structuring element which locally adapts its shape to the image structures. In Fig. 1 is given a toy-example of the effects of the close-holes operator and the area opening.
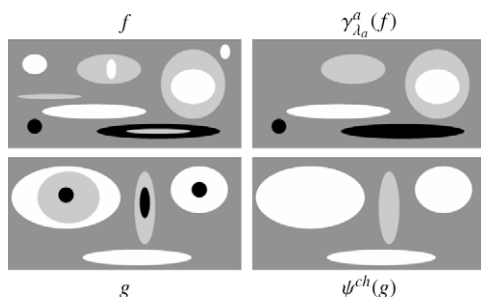
2.3. Generalized grey-level distance function and shortest paths

The generalized distance function (GDF) for grey-level images was first introduced in [7]. The algorithm is based on a modification of the classic two-pass sequential distance function algorithm of [8] so that: (1) edge cost is taken into account; (2) raster and anti-raster scans are iterated until stability. Let us denote by $N^+(p)$ (resp., $N^-(p)$) the neighbors of pixel p scanned before p (resp., after p) in a raster scan, for a 8-connected grid (neighborhood graph). In this graph, to each edge between two neighboring pixels p and q of an image f one associates the cost value $C_f(p, q) = f(p) + f(q)$ (or any other monotonically increasing function, such as $\max(f(p), f(q))$ or $\min(f(p), f(q))$). More specifically, the algorithm of GDF to set X in image f proceeds as follows:

- Initialise result image $d : d(p) = 0$ if $p \in X$ and $d(p) = +\infty$ otherwise.
- Iterate until stability:
  – Scan image in raster order $\rightarrow$ For each pixel p, do: $d(p) \leftarrow \min\{d(p) + \alpha, \min\{d(q) + C_f(p, q), q \in N^+(p)\} + \alpha\}$.
  – Scan image in anti-raster order $\rightarrow$ For each pixel p, do: $d(p) \leftarrow \min\{d(p) + \alpha, \min\{d(q) + C_f(p, q), q \in N^-(p)\} + \alpha\}$.
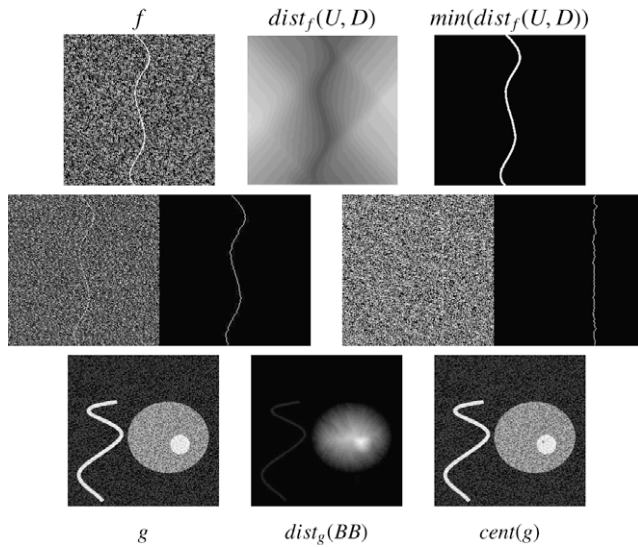
Depending on the cost value considered, the algorithm typically converges in two or three iterations (relatively efficient). The parameter α balances the influence of the geometric distance with respect to the intensity-based distance. In particular, the standard binary distance function is obtained when $C_f(p, q) = 0$ and $\alpha = 1$. Depending on the choice of the set X, two algorithms are considered in this paper: shortest path crossing an image and image centroid.

2.3.1. Global minimal paths, GMP

Each path P in the 8-connect graph has an associated cost $C_f(P)$, equal to the sum of the cost of its successive edges. We can now define the distance $d_f(p, q)$ between two pixels p and q in the image f as: $d_f(p, q) = \min\{C_f(P), P \text{ path between } p \text{ and } q\}$. For the simple problem of finding a path of minimal cost (or global minimal path, GMP) going from the top row U to the bottom row D of the image, we use the following result: a pixel p belongs to such a minimal path if and only if $d_f(p, U) + d_f(p, D) = d_f(U, D)$. This is the approach introduced by [7]. To extract such Up/Down GMP in image f, we can therefore proceed as follows:

- Compute GDF to set U in image f: for each pixel p, compute $d_f(p, U)$.
- Compute GDF to set D in image $f : d_f(p, D)$.
- Add these two distance functions, $d_f(U, D)(p) = d_f(p, U) + d_f(p, D)$.
- Find u_{min}, the minimal value of $d_f(U, D)$ and threshold the result in order to keep only the pixels which values in $d_f(U, D)$ are equal to u_{min}.

The criterion to define the shortest path can be "relaxed" by considering a greater threshold value, $u_{w-path} = u_{min} + N_{paths} - 1$. In such a case, by taking the pixels $\leqslant u_{path}$ and according to the value of N_{paths}, a wide minimal path is obtained. Since the extracted minimal paths are preferentially located on dark pixels (i.e., have low cost), the original image with the bright track must be inverted before computing the two GDFs. From an algorithmic point of view, the problem is reduced to computing two grey-weighted generalized distance transforms. Fig. 2 shows some examples, illustrating the robustness against the noise. To give priority to the "vertical" paths, the computation of the distance function is constrained for raster scan to the top-left, top-middle and top-right

Fig. 1. Top, example of area opening ($\lambda_a = 1000$ pixels). Bottom, example of close-holes operator.

Fig. 2. Top, U/D global minimal path using GDF. Middle, two examples of U/D shortest path detection in very noisy images. Bottom, centroid using GDF.

pixels of p in the neighborhood $N^+(p)$ (resp., bottom-left, bottom-middle and bottom-right for anti-raster scan $N^-(p)$). Another way to formulate it is to say that at any location along a track, according to the neighborhood graph used, it is assumed that the absolute value of the angle between the track and the vertical direction is less than or equal to 45. This guarantees a certain smoothness to the extracted tracks. This segmentation can be interpreted in terms of an optimality criteria framework [7]: (1) the pixel values along the track (to maximize), (2) the length of the track (to minimize), (3) the raggedness of the track (to minimize).

2.3.2. Image centroid

Working in polar coordinates involves the selection of the center (x_c, y_c) for each image, and this is a critical choice. If the selected center point is skewed from the "real" center of the target structure, the analysis in polar coordinates may well be wrong. The optimal (x_c, y_c) can be obtained also with the GDF. The idea is to compute in image f the GDF to the image border set BB, and then to consider that the maximum of the corresponding function includes the grey-level centroid of the image. Being precise, we can proceed as follows:

- Compute GDF to set BB in image f: for each pixel p, compute $d_f(BB)$.
- Find u_{max}, the maximal value of $d_f(BB)$ and threshold the result in order to keep only the pixels which values in $d_f(BB)$ are equal to u_{max}: these pixels define set C.
- If C has more than one pixel, compute the centroid (using binary moments) of set C.

Fig. 2 gives an example of centroid computation. The method is quite robust and it allows detecting the optimal center for embedded structures. Note also that the GDF distance function only takes into account the bright structures. Consequently, if we are interested in the centroid of an object with a large hole, a close-holes operator can be used to compute either the centroid of the object without its hole or the centroid of the hole itself.

3. Algorithm

The iris segmentation algorithm is based in a combination of the above presented morphological tools, working mainly in polar

coordinates. In this section, the different steps are described in detail and illustrated with an iris segmentation example (for which the proposed method performed the best in the NICE-I contest).

3.1. General framework

In Fig. 3 is provided a flowchart representing the main blocks of the proposed algorithm. First, a grey-scale image is selected from the colour image and the reflections are removed. Secondly, a prior segmentation of the external iris border is obtained and afterwards the pupil is segmented. Then, the prior outer iris border segmentation is refined to avoid eyelid and eyelashes artifacts and finally is combined with the binary masks of the pupil segmentation and reflections in order to achieve the final result.

3.2. Colour component selection

Let $\mathbf{f}(x,y) = (f_R(x,y), f_G(x,y), f_B(x,y))$ be the original eye colour image, which is the input to the algorithm. The first step is the selection of the most appropriate grey-level image for the
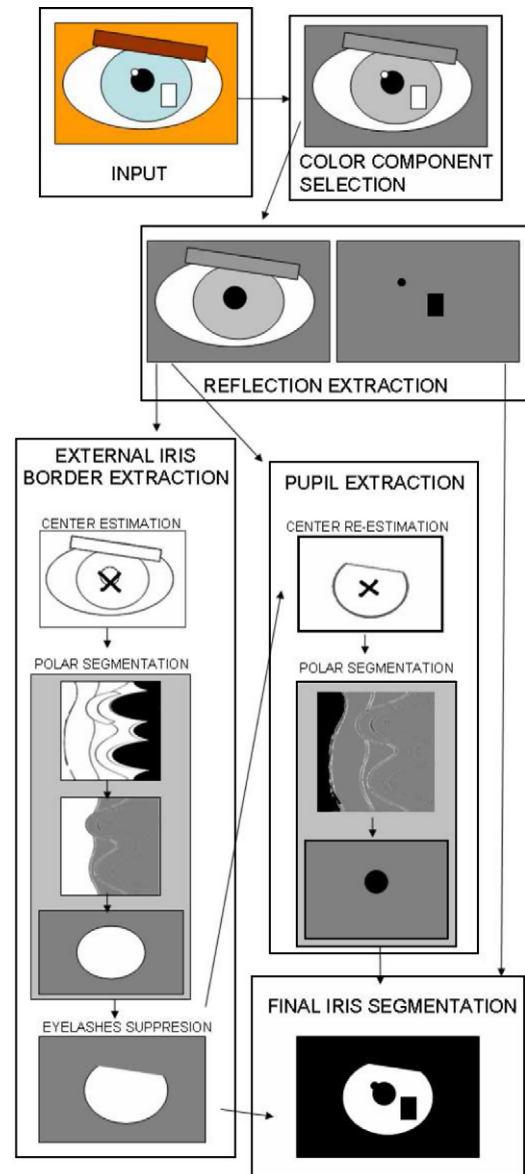
Fig. 3. Schema of the different modules composing the algorithm.

segmentation of the different elements. Based on the hypothesis that the image objects are better "separated" when the image histogram has more information, the selection relies on choosing the R, G or B component which presents the maximal entropy of the histogram, i.e., $f_{eye}(x,y) = f_\xi(x,y)$, where $\xi = \arg_C \max \mathcal{H}(f_C)$.

3.3. Reflection extraction

The specular or diffused reflections appear on the eye image as bright spots of different size and shape which can obstruct the iris texture or to introduce new boundaries for the iris segmentation. Extraction is achieved using the area opening operator. Next, the binary mask of reflections is obtained by thresholding the residue image. We must notice an interesting effect of "inpainting" of the area opening, which interpolates grey values for the removed reflection according to the surrounded structures. Consequently, no new gradients are introduced in the image with this filtering step, see Fig. 4. As we will see later, this property is crucial for the polar segmentation step. The mathematical formulation is as follows:

(1) $\hat{f}_{reflection\text{-}free\text{-}eye} = \gamma^a_{S_{reflex}=800}(f_{eye})$,

(2) $M_{reflex} = T_{u_{reflex}=0.15}(f_{eye} - \hat{f}_{reflection\text{-}free\text{-}eye})$.

3.4. External iris border extraction

In this module, an estimation of the center of the iris is used to transform the image to polar coordinates. A prior segmentation of the iris is obtained performing morphological operators and calculating U/D minimal paths in this space. Finally, the prior segmentation is transformed again into cartesian coordinates and refined in order to suppress eyelid and eyelashes. The output consists in a binary mask of the iris including the pupil.

3.4.1. Center estimation

Contrary to classical approaches for iris segmentation [9], and taking into account the heterogeneity of the image database, our approach for center detection does not rely in the circularity of the iris. In fact, iris images are usually partially occluded or can be off-angle, making the iris shape not always completely circular. Nevertheless, the eye structure is always a embedded structure: skin is darker than sclera, sclera is lighter than iris and iris is lighter than pupil. The close-holes operator applied to the eye image, fills
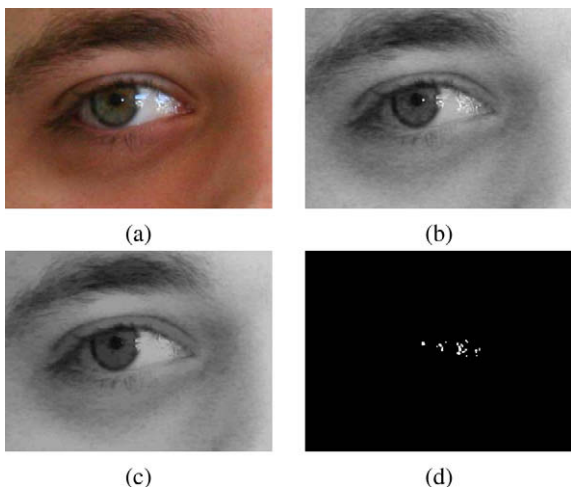
always the embedded structure of the existing part of the sclera–iris–pupil structure. Though it is usually enough to perform a simple close-holes operator, in our algorithm we combined two close-hole operators and image inversions in order to filter the image structure as much as possible, see Fig. 5. The generalized grey-level distance starting from the border of the image is calculated on the residue of the original image and filled image. The distance maximum is chosen as the corresponding center. As iris images are usually centered, we introduced a bias to the center in the calculation of the grey-level distance by taking $\alpha = 1$. This is the mathematical formulation of the algorithm steps:

(1) $f_{cent\ 1} = (\hat{f}_{reflection\text{-}free\text{-}eye})^c$.

(2) $f_{cent\ 2} = \psi^{ch}(f_{cent\ 1})$.

(3) $f_{cent\ 3} = (f_{cent\ 2})^c$.

(4) $f_{cent\ 4} = \psi^{ch}(f_{cent\ 3}) - f_{cent\ 3}$.

(5) To compute $dist^{\alpha=1}_{f_{cent\ 4}}(BB)$ and to assign for (x_c, y_c) the max of the distance function.

3.4.2. Polar segmentation

The image is transformed into polar coordinates using the estimated center (x_c, y_c). The polar transformation of the function $f(x,y)$ generates a new function image $f^\circ(\rho,\omega) : E_{\rho,\omega} \to \mathcal{T}$, where the support of the image is the space $E_{\rho,\omega}, \hat{\eta} = (\rho,\omega) \in (Z \times Z_p)$ and where the angular variable $\omega \in Z_p$ is periodic with period p equivalent to 2π. A new relation of neighborhood is established between points at the top of the image ($\omega = 0$) and the ones at the bottom of the image ($\omega = p - 1$). Therefore, the image can be seen as a strip where the superior and the inferior borders are joined. Before performing the corresponding morphological operators, we extended the image along its angular direction by adding the top part of the image onto the bottom and the bottom part onto the top. Rendering the image cyclic avoids possible edge effects and allows us to calculate the circular minimal paths. We assume that the iris region is a connected component that covers the center point. The closed contour delimiting this region is an almost
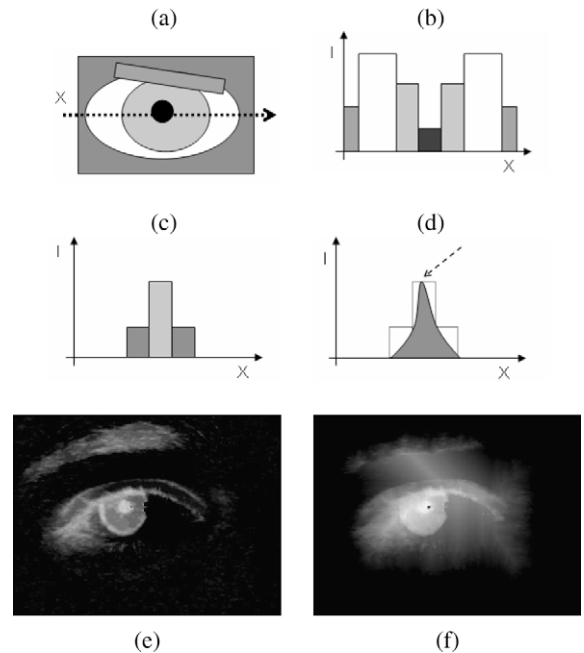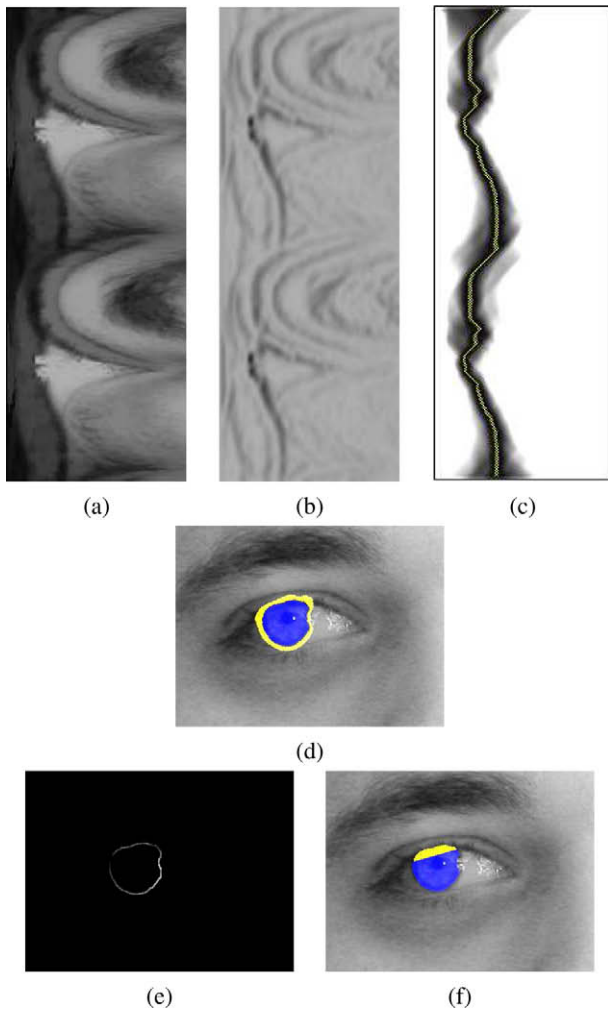

Fig. 5. Diagram of center detection: (a) input image; (b) intensity projection of x-axis; (c) residue from close-holes operated on (b); (d) grey-level generalized distance on (c), arrow indicates the maximum value. (e) residue of close-holes operators on the eye image. (d) Generalized grey-level distance on (a); in blue the maximum of the generalized distance, corresponding to the detected center.

Fig. 4. (a) Original input image; (b) colour component selection:red channel; (c) reflection-free image; (d) reflections binary mask.

vertical path in the polar space that follows the well defined gradient corresponding in the ideal case to the transition sclera–iris or in the remaining cases to the transition skin–iris or eyebrows–iris. Before calculating this minimal path, a morphological multiscale gradient is performed in polar coordinates and is then smoothed by an anisotropic averaging filter (i.e., sizes in radial and angular dimensions are different). After calculating the U/D generalized grey-level distance, a set of minimal paths is transformed back to the cartesian space. The iris corresponds to the region inside the transformed paths (see Fig. 6). Hereafter the mathematical formulation of the algorithm steps:

(1) $\hat{f}_{reflection\text{-}free\text{-}eye}(x,y) - \rightarrow \hat{f}^{\circ}_{eye}(\rho,\omega)$, with $-\pi \leqslant \omega \leqslant 3\pi$ (ω is discretized in 180 pixels), $0 \leqslant \rho \leqslant R^{max}$ (typically $R^{max} = Y^{max}/2$, where Y^{max} is the image size in vertical dimension).

(2) $\hat{f}^{\circ}_{grad} = \left(f^{\circ}_{eye} - \varepsilon_{B_{\rho=5,\omega=5}}\left(\hat{f}^{\circ}_{eye} \right) \right) + \left(\hat{f}^{\circ}_{eye} - \varepsilon_{B_{\rho=5,\omega=10}}(\hat{f}^{\circ}_{eye}) \right).$

(3) $\hat{f}^{\circ}_{grad} = \mathrm{Mean}_{B_{\rho=3,\omega=6}}(f^{\circ}_{grad}).$

(4) To compute $dist^{\alpha=0}_{f^{\circ}_{grad}}(U,D)$.

(5) To find the min value u_{min}, and to threshold with $N_{paths} = 500$ obtaining the wide minimal path in f°_{paths}.

(6) $f^{\circ}_{paths}(\rho,\omega) \rightarrow f_{paths}(x,y)$.

(7) $\hat{f}_{paths} = \varphi B_2(f_{paths})$ (to avoid open contours).

(8) $M^{prior}_{iris} = y^{rec}((\hat{f}_{paths})^c, mrk(x_c,y_c)))$, where $mrk(x_c,y_c)$ is the image of iris center.

3.4.3. Eyelid and eyelashes suppression

As we mentioned before, the upper part of the iris is sometimes occluded by eyelid and eyelashes. Thus, the transition (gradient) to be taken into account for the correct segmentation is not only from sclera to iris, but also from a fuzzy region composed by eyebrows, eyelashes and skin to iris. The prior segmentation presented in the previous section follows a path that combines circularity and gradient information, but it is not always accurate in the upper regions of the iris, where limits are not so well defined. For this reason, we introduced a very simple model that refines this segmentation. The idea is to "cut" the top part of the prior segmentation with a straight line. This line passes by two points that are chosen from a virtual contour placed some pixels outside of the prior segmentation. The transition of this contour from sclera to the top part of the iris (eyebrows, eyelashes and skin) in left and right sides defines the cutting line. The algorithm works as follows (see example in Fig. 6):

(1) To extract an inner contour of the mask iris at a distance of 7 pixels, i.e., $C_{iris} = \delta_{B7}(M^{prior}_{iris}) - \delta_{B5}(M^{prior}_{iris})$.

(2) Using the horizontal going through the iris center, to decompose the contour into two parts, i.e., $C_{iris} = C^{up}_{iris} \cup C^{down}_{iris}$.

(3) The upper part contour is valued with the intensity of iris image, i.e., $f_{ctu\ iris}(\mathbf{x}) = \hat{f}_{eye}(\mathbf{x})$ if $C^{up}_{iris}(\mathbf{x}) = 1$, otherwise $f_{ctu\ iris}(\mathbf{x}) = 0$.

(4) The intensities of $f_{ctu\ iris}$ are normalized in the interval 0–1, then the image is thresholded at value u_{occlu} to obtain the partial contour $\widehat{C}^{up}_{iris}$, typically $u_{occlu} = 0.3$.

(5) $\mathbf{M}^{occlu}_{iris} = \mathrm{ConvexHull}(C^{down}_{iris} \cup \widehat{C}^{up}_{iris})$.

(6) $\mathbf{M}^{refin}_{iris} = \mathbf{M}^{prior}_{iris} \cap \mathbf{M}^{occlu}_{iris}$.

Although it is a very simple model that does not follow precisely eyebrows and eyelashes artifacts – which are sometimes, especially in dark irises, not even easy to spot for humans – it provides a very good trade-off between simplicity/robustness and accuracy.

3.5. Pupil extraction

The pupil is segmented with a similar procedure to the outer iris border extraction. First, the pupil center is refined using the close-holes operator and grey-level generalized distance from the prior iris segmentation. The pupil is then segmented using the circular minimal-path obtained from the polar transformation of the reflection-free image.
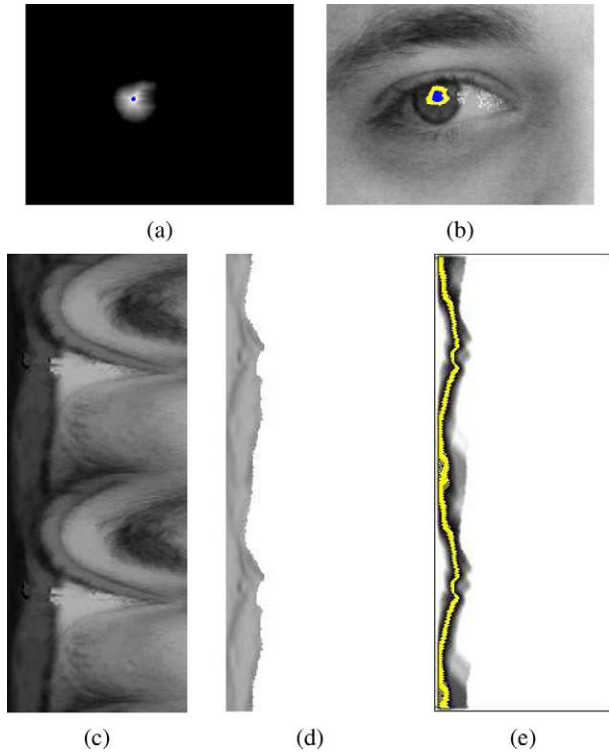
3.5.1. Center estimation

In order to find the pupil center, we worked only in the iris region selected by the prior iris segmentation. The close-holes operator is performed and the grey-level distance is calculated on its residue with no bias to the center in its metric, see Fig. 7a. The algorithm is as follows:

(1) $\hat{f}_{iris}(\mathbf{x}) = \hat{f}_{reflection\text{-}free\text{-}eye)}(\mathbf{x})$ if $\mathbf{M}^{prior}_{iris}(\mathbf{x}) = 1$, otherwise $\hat{f}_{iris}(\mathbf{x}) = 0$.

(2) $f_{cent\ pup} = \psi^{ch}(\hat{f}_{iris}) - \hat{f}_{iris}$.

(3) To compute $dist^{\alpha=0}_{f_{cen\ pup}}(BB)$ and to take for (x^{pup}_c, y^{pup}_c) the max of the distance function.

3.5.2. Polar segmentation

The reflection-free image is transformed in to its polar coordinates using the center (x^{pup}_c, y^{pup}_c) and the U/D minimal paths are

Fig. 6. (a) Cycled polar transformation of eye image; (b) negative of multiscale morphological gradient of (a); (c) U/D generalized distance of (b), the yellow line corresponds to the minimal circular path; (d) in yellow, transformation to cartesian coordinates of (b) and in blue, selected prior iris segmentation. (e) Normalized contour outside the prior iris segmentation; (f) in blue refined iris segmentation and in yellow suppressed part of the prior segmentation.

Fig. 7. (a) Generalized distance function for pupil center detection and maximum in blue; (b) cycled polar transformation of eye image centered in maximum of (a); (c) multiscale gradient constrained to iris prior segmentation boundaries; (d) U/D generalized distance of (c), the yellow line corresponds to the minimal circular path; (e) segmentation of pupil in blue and border in yellow.

Fig. 8. Examples of algorithm execution: in blue final segmentation, in red pupil segmentation, in green extracted reflections and in yellow the suppressed part of prior segmentation.
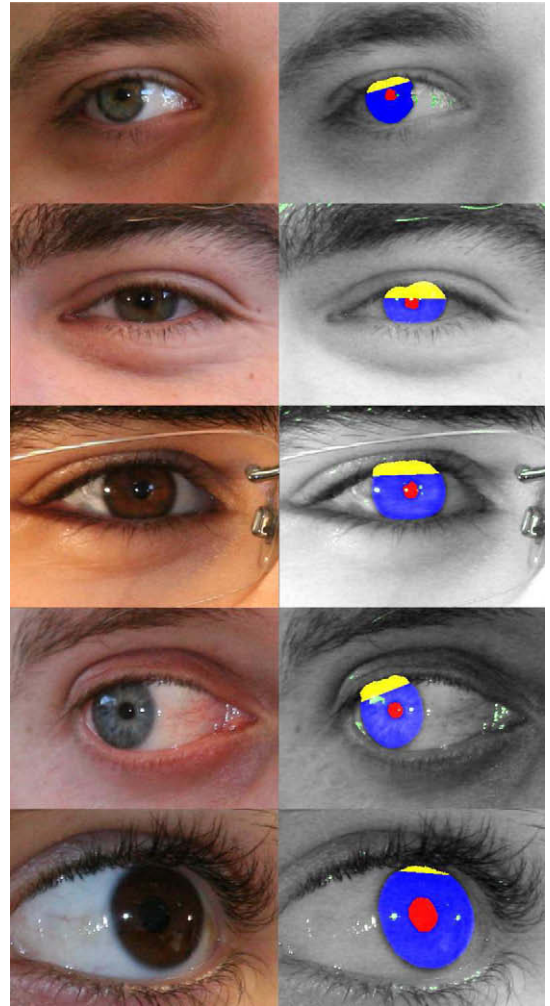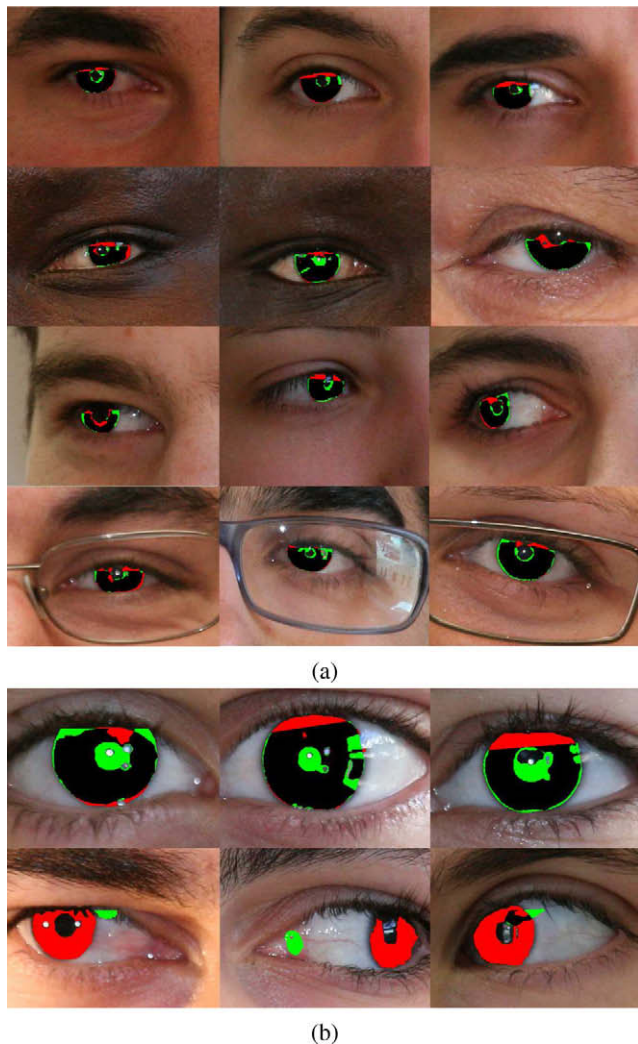
calculated in the same way than in the outer iris segmentation. The only modification is that these minimal paths are radially constrained into $[r_{min}, r_{max}]$, where r_{max} is given by $0.8 \times$ radius of the prior iris segmentation and r_{min} is fixed to 5 pixels for inconsistency reasons of the central point (note that for $r = 0$, all the pixels have the same value in the polar representation). Taking into account the radial boundaries, the algorithm is the same as for outer iris segmentation (the value for N_{paths} is set to 50), see illustrative example in Fig. 7. The output of this module is the binary mask of the segmented pupil in cartesian coordinates: M_{pupil}.

3.6. Combination of different binary masks and final segmentation

The complete segmentation is given by the refined outer iris mask minus the reflections and the pupil masks; i.e, $M_{iris} = M_{iris}^{refin} \setminus (M_{reflex} \cup M_{pupil})$ This modular paradigm minimizes errors. We introduced a final security module concerning the maximal size allowed to the iris ($a_{iris}^{max} = 35,000$ pixels) in case the outer border segmentation has an improbable size or the minimal circular path algorithm did not find convergence; i.e., if $\text{Area}(M_{iris}) > a_{iris}^{max} \Rightarrow M_{iris} = \emptyset$. See the final segmentation of the presented example and other examples of the results of the different segmentation modules in Fig. 8.

3.7. Parameters optimization

Algorithm parameters were optimized using a 200 computer cluster (Core2Duo 2 GHz). Each parameter was permitted to vary between three and five different values previously manually chosen. The parameters for external iris segmentation were exhaustively tested. The parameters that gave the best results were retained in order to exhaustively test the pupil segmentation

module. These computations allowed us to find the best set of parameters for each image and the set of parameters that performed best globally in the testing dataset. These parameters were fixed in the algorithm submitted to the contest and are the ones described in this paper.

4. Result analysis and discussion

The NICE-I error measure $E1$ (i.e., the proportion of correspondent disagreeing pixels between the manually corrected image and the algorithm output) is 0.028 for the training dataset and 0.0301 for the testing dataset. These results were obtained with the optimized fixed algorithm parameters. In fact, several parameter sets give the same result $E1 = 0.028$ and an heuristic intuitive choice of parameters gives similar results. Parameters are mainly function of image size and can be fixed *a priori* depending on the acquisition characteristics. We notice that the proposed method is quite independent of the database size concerning the optimization stage. It has a very robust behavior, performing in a similar manner for very different kinds of images. The simple model used to suppress eyelid and eyelashes artifacts is not very precise, but it works in a very consistent and controlled way. Concerning the algorithm limits with this implementation and the tested parameters set, we obtained $E1 = 0.022$ using the best possible parameters

(a)

(b)

Fig. 9. Examples of images where the proposed algorithm performed (a) better or (b) worse than the rest of NICE-I participants (in red false negatives and in green false positives).

and consequently, in a very fast algorithm we can fix $f_{eye}(x,y) = f_R(x,y)$. Other more advanced colour preprocessing can improve the grey-level image selection, typically by selecting between the colour invariant components [10]. As an example, in order to improve pupil segmentation, each image was processed using the red component and the saturation component for the pupil segmentation. Error $E1$ in the training set calculated from the best of the two segmentations in each image is 0.025. One possibility in order to improve results could be to introduce a previous classification module that choose the correct parameters for each image depending on its characteristics (iris colour, glasses, off-angle iris, skin, ...), but this possibility should be studied carefully because a classification stage may also introduce errors. In this sense, first tests with a neural network applied to the 3D colour histogram shows interesting classification properties. However, a larger training database is probably needed in order to characterize rare circumstances such as when hair is in front of the eye.

5. Conclusions

We have proposed a new approach for fast iris segmentation that relies on the closed nested structures of iris anatomy (the sclera is always brighter than the iris, and the iris is always brighter than the pupil) and its polar symmetry. The proposed method applies mathematical morphology for polar/radial-invariant image filtering and feature extraction and for circular segmentation using shortest paths from generalized grey-level distances. Results on the NICE-I iris contest placed the algorithm among the finalists and showed very robust behavior, especially when dealing with half-closed eyes, different skin colours/illumination or subjects wearing glasses. Further developments using this kind of approach or its combination with classical methods look to be an open and promising field.

Acknowledgements

References

[1] J. Matey, Iris image segmentation and sub-optimal images, Image Vis. Comput. J., in this issue, 28(2) (2010) 215–222.
[2] M.A. Luengo-Oroz, J. Angulo, Cyclic mathematical morphology in polar-logarithmic representation, IEEE Trans. Image Process. 18 (5) (2009) 1090–1096.
[3] J. Angulo, Polar modelling and segmentation of genomic microarray spots using mathematical morphology, Image Anal. Stereol. 27 (2008) 107–124.
[4] H. Proenca, L.A. Alexandre, The NICE-I: Noisy Iris Challenge Evaluation – Part I, in: IEEE International Conference on Biometrics: Theory, Applications, and Systems, 2007, BTAS, 2007, pp. l–4.
[5] J. Serra, Image Analysis and Mathematical Morphology, vol. I, and Image Analysis and Mathematical Morphology, vol. II: Theoretical Advances, Academic Press, London, 1982, 1988.
[6] L. Vincent, Morphological area openings and closings for grayscale images, in: Proceedings of NATO Workshop Shape in Picture, Driebergen, Holland, September 1992.
[7] L. Vincent, Minimal path algorithms for the robust detection of linear features in gray images, in: Proceedings of International Symposium on Mathematical Morphology (ISMM'98), Kluwer, Amsterdam, 1998, pp. 331–338.
[8] A. Rosenfeld, J. Pfaltz, Distance functions on digital pictures, Pattern Recognit. 1 (1968) 33–61.
[9] J. Daugman, High confidence visual recognition of persons by a test of statistical independence, IEEE Trans. Pattern Anal. Mach. Intell. 15 (11) (1993) 1148–1161.
[10] Th. Gevers, A.W.M. Smeulders, Color based object recognition, Pattern Recognit. 32 (3) (1999) 453–464.

choice for each image. The fact that the circular shape of iris does not play a critical role in the center detection neither in the segmentation, makes the algorithm suitable for non-ideal images. The proposed algorithm performed better than the rest of the NICE-I finalists (see Fig. 9) in several half-closed eyes, medium off-angle irises, dark skin people and people wearing glasses (the algorithm is robust to different skin colours or the presence of glasses). On the other hand, the algorithm achieved worse results than the other participants (see Fig. 9) for some extreme off-angle iris – when the center is not correctly detected – and in some easy images with circular shapes for iris and pupil, where the algorithm did not obtain a perfect segmentation because of the cut in the top of the iris and/or a dizzying or inconsistent pupil segmentation when a dark iris. Current non-optimal implementation in MATLAB takes around 3 s per image segmentation in a common PC (Core2-Duo 2.33 GHz). Nevertheless, computational time can be drastically reduced since there is no exhaustive computation and the code can be easily optimized.

The main information that remains to be exploited by the algorithm is colour. In general, we have observed from the training examples that the best component corresponds to the red one